Appl. Phys. B 73, 535–540 (2001)
DOI: 10.1007/s003400100704

Applied Physics B
Lasers and Optics

B. OSTER
H. FOUCKHARDT✉

M-waveguide structures for direct phase matching in AlGaAs

AG Integrierte Optoelektronik und Mikrooptik, Fachbereich Physik, Universität Kaiserslautern, Erwin-Schroedinger-Straße, 67663 Kaiserslautern, Germany

Received: 16 May 2001/Revised version: 2 August 2001
Published online: 23 October 2001 •

ABSTRACT In this paper the potential of M-waveguide structures for direct phase matching in AlGaAs is investigated by numerical simulations. Principal waveguiding characteristics are discussed. The impact of the optical layer thicknesses is analyzed with respect to phase matching and conversion efficiency for second harmonic generation (SHG). An optimization of the M-waveguide parameters yields a normalized conversion efficiency of 153 or 214 %/W respectively.

PACS 42.79.Gn; 42.79.Nv; 85.30.De

1 Introduction

Thin waveguide films in integrated optics offer an interesting alternative for optical frequency conversion compared to conventional bulk devices. High intensities can be guided over relatively long path lengths, making waveguides predetermined for nonlinear interactions such as second harmonic generation (SHG). Critical phase matching can be overcome in waveguides by equating the effective indices of the fundamental and harmonic wave [1], resulting in direct phase matching. Different approaches for phase matching applied in waveguides are, for example, Cerenkov radiation phase matching [2] and quasi phase matching [3]. So far mostly birefringent waveguides [4] have been applied for direct phase matching. Another possibility for obtaining the same effective indices at the frequencies ω and 2ω is to utilize the waveguide dispersion in order to compensate for the material dispersion. Especially in this case a large nonlinear interaction overlap of the involved fields combined with a material of high nonlinear susceptibility is required to obtain efficient guided wave frequency conversion.

Principally two waveguiding mechanisms can be distinguished: conventional guiding by total internal reflection (TIR) and leaky waveguiding due to Fabry–Perot reflections (operating in antiresonance). Antiresonant reflecting optical waveguides (ARROWs) [5–8] show a characteristic waveguide dispersion behavior. This contribution deals with the possibility of using the distinctive ARROW dispersion characteristics for direct phase matching.

✉ Fax: +49-631/205-4147, E-mail: fouckhar@physik.uni-kl.de

We chose AlGaAs as the material system. It is a promising candidate for devices in integrated optics. It is easy to process and allows integration by wafer fusion with AlGaAs laser sources. Moreover, it has a high nonlinear susceptibility, but also a strong material dispersion in the near infrared. For an SHG experiment a laser source at 1.55 μm can be applied, because the harmonic wavelength will still lie above the bandgap wavelength for Al fractions larger than 30%.

As a result of numerical simulations we obtained an ARROW-M-waveguide as one variation of an M-shaped refractive-index profile allowing direct phase matching. Another variation has been recently suggested in [9] for the $LiNbO_3$ material system. Our simulations show that the M-waveguide, which is a derivation of a symmetric single-cladding ARROW, can be operated either as an ARROW structure or as a coupler structure [10]. In this paper we generally discuss the different M-waveguide structures with respect to direct phase matching in AlGaAs. The M-waveguide structures are compared with regard to waveguiding aspects and optimized in consideration of frequency conversion efficiency. The optimized device yields a normalized conversion efficiency of 153 or 214%/W respectively.

2 Theoretical background

In a second harmonic process inside a waveguide of an optical nonlinear material such as GaAs, a nonlinear polarization is generated and there will be a nonlinear interaction of the fundamental mode field at frequency ω and the harmonic mode field at 2ω. The normalized nonlinear overlap integral K of the interacting mode field distributions $E_i(x, y)$ of the fundamental wave at ω and the harmonic wave at 2ω is calculated as follows:

$$K = \frac{\left|\iint_{-\infty}^{+\infty} E_\omega^2 \, E_{2\omega} \mathrm{d}x\mathrm{d}y\right|}{\iint_{-\infty}^{+\infty} E_\omega^2 \mathrm{d}x\mathrm{d}y \left(\iint_{-\infty}^{+\infty} E_{2\omega}^2 \mathrm{d}x\mathrm{d}y\right)^{\frac{1}{2}}} . \quad (1)$$

This formula is used in order to compare the presented M-waveguide designs to the M-waveguide approach as first suggested by Chowdhury and McCaughan [9]. However, for slab waveguide designs with varying nonlinear susceptibility in the plane perpendicular to the layers $d_{ijk} = d(x)$, the function $d(x)$ needs to be considered in the integral of the numera-

tor [11] [see (5) and (6)]. With K an effective interaction area F_{eff} can be defined according to [4]:

$$F_{\text{eff}} = \frac{1}{K^2} \,. \tag{2}$$

This way the normalized conversion efficiency η_{nor} for a waveguide of the length L can be expressed as

$$\eta_{\text{nor}} = \frac{P(2\omega)}{P^2(\omega)} = \frac{8\pi^2\, d_{\text{eff}}^2}{\varepsilon_0 c \lambda_\omega^2 n_{\text{eff}}^2(\omega) n_{\text{eff}}(2\omega)} \cdot \frac{L^2}{F_{\text{eff}}} \,. \tag{3}$$

The phase-mismatch term $\text{sinc}(\Delta kL/2)$ is already neglected, since direct phase matching is assumed. For the effective nonlinear coefficient $d_{\text{eff}} = \chi^{(2)}/2$ (expressing $\chi^{(2)}$ as a scalar quantity), a mean square value over all layers is determined for a layer structure with different $\chi^{(2)}$-value per layer. The mean-square value takes into account the fact that the magnitude of $\chi^{(2)}$ in AlGaAs is expected to decrease with Al concentration [12]. For each layer the squared d coefficient is weighted by the layer thickness, and the mean value is scaled by the thickness of the whole layer structure. For an N-layer stack having layer thicknesses $h_1 \ldots h_N$ with different Al concentrations $x_1 \ldots x_N$, the "average" nonlinear d coefficient d_{eff} is calculated as follows:

$$d_{\text{eff}}^2 = \frac{d_{x_1}^2 h_1 + d_{x_2}^2 h_2 + \ldots + d_{x_N}^2 h_N}{h_1 + h_2 + \ldots + h_N} \,. \tag{4}$$

To calculate the effective indices n_{eff} a standard transfer matrix algorithm [13] is employed.

3 Numerical results

Direct phase matching shows up in the dispersion diagrams as crossing points of the dispersion curves of different modes of the fundamental wave at λ and the harmonic wave at λ/2. For the appropriate mode fields the overlap integral K can be calculated. Subsequently the conversion parameters can be determined according to (2)–(4). As the fundamental wavelength we chose $\lambda = 1.6\,\mu\text{m}$. For all simulations transverse electric (TE) polarization is used.

3.1 *Potential of ARROWs for direct phase matching*

ARROWs are based on the leaky guiding of waves due to very strong multiple Fabry–Perot reflections at glancing incidence at the layers adjacent to the core layer. Therefore those layers are called reflectors or claddings. This way, the wave can also be guided in a semiconductor core area of low core index. Lateral index profiles for two ARROW structures are illustrated in Fig. 1. Figure1a shows a symmetric ARROW with one reflector layer on each side of the core. Figure1b illustrates an asymmetric ARROW with TIR as the guiding mechanism on one side of the core and ARROW guiding on the other side of the core. However, even for the latter case, the dispersion behavior is determined by the ARROW guiding.

Due to their characteristic index profiles, ARROWs have distinctive waveguide dispersion [14]. In Fig. 2 the effective

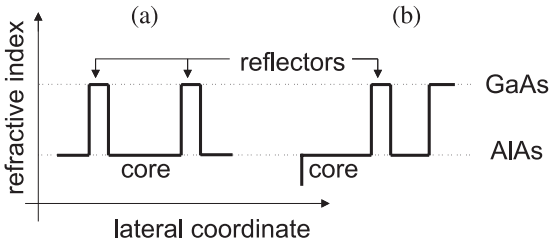

FIGURE 1 ARROW structures in the AlGaAs material system: (a) symmetric single cladding ARROW; (b) asymmetric ARROW structure

index is shown versus the reflector thickness for the asymmetric layer structure of Fig. 1b. The solid curves belong to the fundamental wave, and the dashed curves to the harmonic wave. There are flat parts, where ARROW modes exist, and steep parts, where reflector modes are supported. For the leaky ARROW modes the wave is mainly propagating in the core layer and the effective index lies below that of the refractive index of the core. For the reflector modes, which are TIR modes, the wave is guided in the reflector layer and, therefore, the effective index will lie between the refractive index of the core and that of the reflector layer.

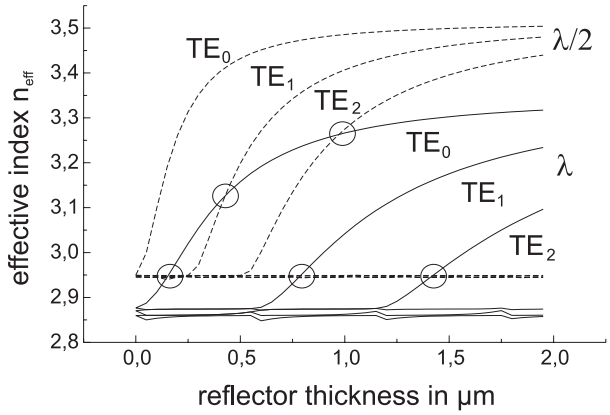

FIGURE 2 Effective index curves versus reflector thickness for the ARROW structure of Fig. 1b. The thickness of the core is 6 μm; *solid lines*: fundamental wavelength (here λ is 2 μm), *dashed lines*: second harmonic wavelength. *Circles* indicate possible direct phase matching points

The circles indicate intersections of the curves for the fundamental (solid) and harmonic (dashed) waves with different combinations of ARROW and reflector modes of different mode numbers. At each intersection the effective index is the same for the fundamental wavelength at λ and the harmonic wavelength at λ/2. Therefore, each of those points represents a possible direct-phase-matching point. However, not all mode combinations are suitable for direct phase matching, because the nonlinear interaction overlap might be too poor or the waveguide losses too high. An ARROW structure for direct phase matching has to fulfil the requirements of high interaction overlap and good confinement in order for an efficient wavelength conversion to be obtained. A better nonlinear overlap could be achieved by the transition to a symmetric structure, and a better confinement by a TIR superstructure.

3.2 *M-waveguide structures for direct phase matching*

The index profile given in Fig. 3, which is a mixture of a TIR superstructure and an ARROW core area, was developed.

It is a derivation of the symmetric single-cladding ARROW (compare Fig. 1a). The superstructure causes a high confinement of the wave, and the symmetry yields a good overlap of the interacting mode fields. The larger fundamental wave at λ is guided in the larger superstructure at the higher refractive index, whereas the smaller harmonic wave at $\lambda/2$ is guided in the smaller ARROW core area at the lower refractive index. This way the material dispersion can be compensated.

Depending on the layer parameters chosen, the waveguide shown is either an ARROW structure or a TIR coupler structure (Fig. 4). A similar TIR coupler structure has been recently published by Chowdhury and McCaughan, who called this waveguide profile M-structure and who were the first to suggest the M-shaped index profile for direct phase matching in $LiNbO_3$ [9]. For the ARROW structure (with thin reflector layers) the core determines the waveguiding and the effective index lies below the refractive index of the core (Fig. 4a). For the TIR coupler structure (with thicker reflector layers) the reflectors determine the waveguiding and the effective index lies above the refractive index of the core and below that of the reflectors (Fig. 4b). The obtained mode fields are supermodes and consist of two coupled reflector modes.

In order to demonstrate the dispersion behavior of the M-waveguide the reflector layer thickness is varied for a fixed core layer thickness for the layer structure given in Fig. 5.

There are two intersection points where the dispersion curve of the fundamental wave crosses a dispersion curve of an even TE mode (index 0, 2 or 4) of the harmonic wave. Those two points are direct phase matching points. For point **A** there is an interaction of a TE_0 pump field with a TE_2 mode field of the second harmonic. Point **B** stands for a TE_0–TE_4 interaction. Both points correspond to two waveguide structures. For the case of the dispersion diagram as shown in Fig. 5, point **A** corresponds to an ARROW structure, whereas point **B** represents a TIR coupler structure.

The impact of the variation of the reflector thickness on the M-waveguide dispersion is clarified when the evolution of the respective mode fields is analyzed. For the larger fundamental wavelength at λ (heavy solid line in Fig. 5) the change of the transverse mode profiles is illustrated in Fig. 6. The core region determines the waveguiding predominantly for $h_1 < h$, and a Gaussian fundamental mode field is obtained

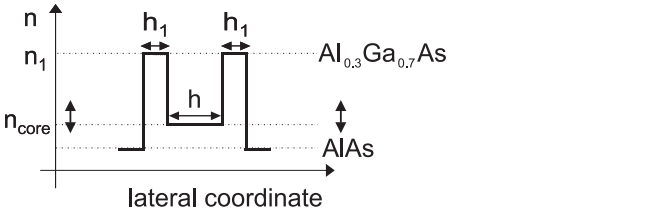

FIGURE 3 M-waveguide index profile with core thickness h and reflector layer thicknesses h_1 in the AlGaAs material system

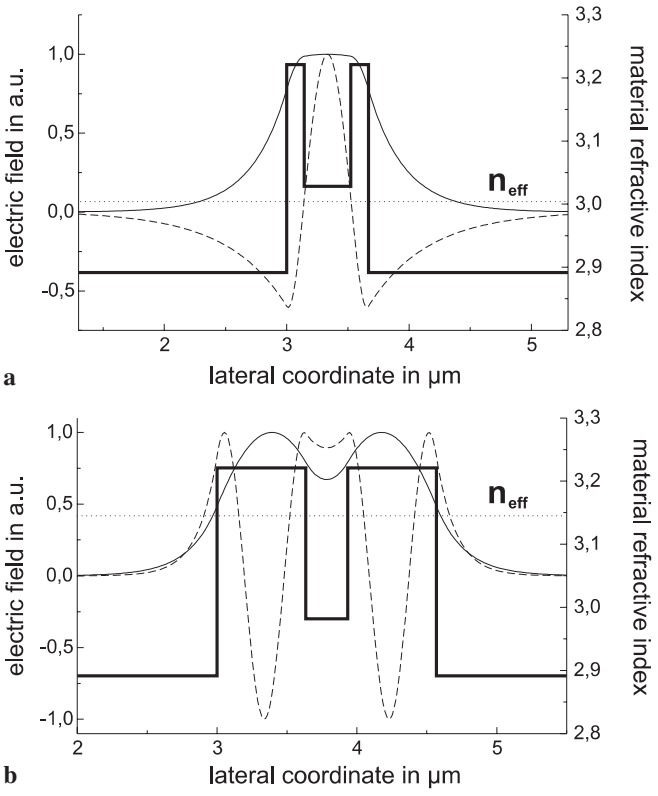

FIGURE 4 M-waveguide variations: index profiles and corresponding mode fields (*solid lines*: fundamental wavelength, *dashed lines*: second harmonic wavelength). **a** ARROW structure, **b** TIR coupler structure

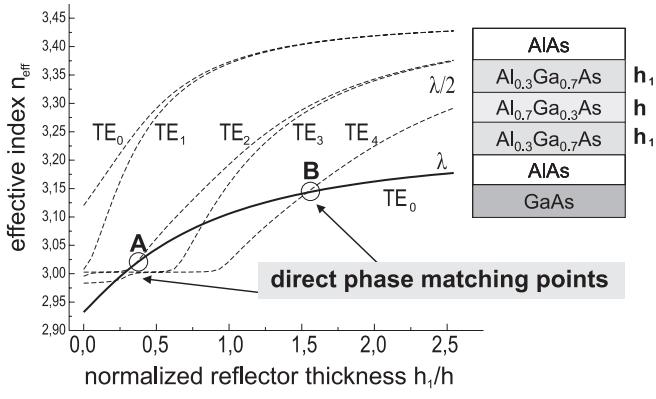

FIGURE 5 M-waveguide dispersion behavior for the given AlGaAs layer structure. Substrate: GaAs; outer reflector layers: AlAs (*thickness* $= 2\,\mu$m); inner reflector layers: $Al_{0.3}Ga_{0.7}As$; central core layer: $Al_{0.7}Ga_{0.3}As$ (thickness $h = 0.385\,\mu$m). *Heavy solid line*: fundamental wave at λ; *dashed lines*: harmonic wave at $\lambda/2$

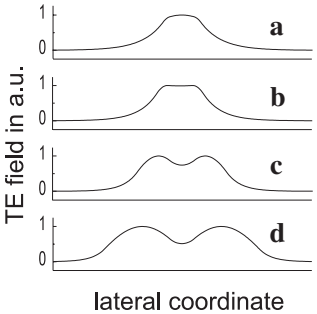

FIGURE 6 Evolution of the TE_0 mode fields of the fundamental wave dispersion curve of Fig. 5 for $h_1/h =$ **a** 0.26, **b** 0.44, **c** 1.3 and **d** 2.6

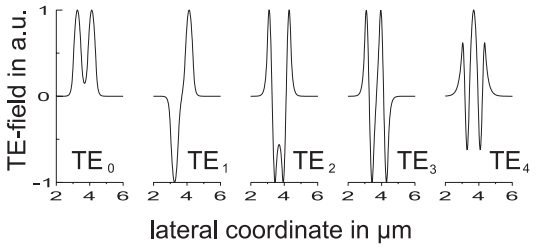

FIGURE 7 TE_0–TE_4 mode fields of the harmonic wave for $h_1/h = 1.3$ in Fig. 5

(Fig. 6a,b). With increasing reflector size, the core evolves into a disturbance of the superior TIR structure manifested in a dip in the middle of the mode profile (Fig. 6c,d). Now the wave must be interpreted as a supermode consisting of two fundamental reflector modes. For $h_1 \gg h$ the coupling character vanishes.

For the smaller harmonic wavelength at $\lambda/2$, the obtained mode fields are shown in Fig. 7 for a fixed reflector size. Since the reflector size is about the same size as that of the core, there is an obvious coupling between the reflector modes. The TE_0–TE_3 mode fields therefore correspond to supermodes. The effective index lies above the refractive index of the core. For the TE_4 mode field, however, the effective index lies below that of the core and an ARROW mode is obtained (compare mode field at the right-hand edge of Fig. 7).

3.3 *M-waveguide optimization*

In order to optimize the waveguide parameters, both the thickness and refractive index of the core layer are varied step by step: $h = 0.2$ to $0.7\,\mu$m, $n_{\text{core}} = n(\text{AlAs})$ to $n(Al_{0.3}Ga_{0.7}As)$ in steps of 10% Al fractions.[1] The refractive indices for the reflector layers are fixed: that of AlAs for the outer reflector layers and that of $Al_{0.3}Ga_{0.7}As$ for the inner reflector layers (compare Fig. 3). The thickness of the outer reflector layers is also fixed at $2\,\mu$m. For each parameter pair (n_{core}, h) direct-phase-matching points are determined by variation of the reflector layer thickness (between 0 and $1\,\mu$m). Then the frequency conversion parameters (1)–(4) are calculated in order to determine η_{nor}. Next, one parameter is changed (either h or n) and the phase-matching points and conversion parameters are derived until an optimum value for η_{nor} is found. This way the obtained lateral index profiles vary between that of a single-cladding ARROW structure (as shown in Fig. 1a) and that of a simple TIR structure.

As expected the TE_0–TE_2 interaction (point **A** in Fig. 5) yields higher values for the overlap integral, whereas the TE_0–TE_4 interaction (point **B** in Fig. 5) yields a higher mean nonlinear coefficient. For Al fractions up to 80%, only coupler structures are found. For an Al fraction of 70% and less, both regimes exist: ARROW and coupler structures, depending on the layer parameters. The best conversion parameters are found for an Al fraction of the core of 70% (compare layer structure on the right-hand side of Fig. 5).

[1] For the $Al_xGa_{1-x}As$ material system the refractive index is determined by the Al fraction x. The higher the Al content, the lower the refractive index.

For the TE_0–TE_2 interaction, the optimized ARROW structure with a normalized conversion efficiency of $\eta_{\text{nor}} = 103\%/\text{W}$ for a device length $L = 1$ cm is shown in Fig. 8. For this structure the ARROW criterion is fulfilled for both λ and $\lambda/2$; the effective index lies below the refractive index of the core. Accordingly the mode field of the fundamental wave corresponds to a spatial fundamental ARROW mode and the mode field of the harmonic wave to a second-order ARROW mode. The waveguide and corresponding conversion parameters are listed in Table 1. The optimized TIR coupler structure for the same nonlinear mode interaction (TE_0–TE_2) yields a best normalized conversion efficiency of $\eta_{\text{nor}} = 153\%/\text{W}$ (for $L = 1$ cm). For this structure the mode profiles basically resemble those of Fig. 8. However, for the fundamental wavelength the reflectors determine the waveguiding; therefore, the mode profile at λ shows a small dip in the middle and the effective index lies above the refractive index of the core (compare Table 1). The large interaction overlap results in the highest normalized conversion efficiency found in our calculations (compare Table 1).

For the TE_0–TE_4 interaction, the ARROW structures yield small values for the nonlinear overlap, so that the normalized conversion efficiencies lie around 10%/W despite large mean nonlinear coefficients of about 90 pm/V. For this interaction the optimized TIR coupler structure corresponds to the M-

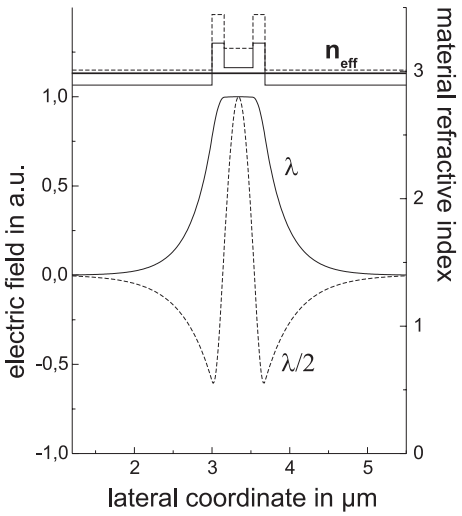

FIGURE 8 Optimized ARROW structure and mode fields for the TE_0 – TE_2 interaction. *Solid lines*: fundamental wave at λ; *dashed lines*: harmonic wave at $\lambda/2$

	ARROW	TIR coupler
Core thickness (µm)	0.37	0.28
Reflector thickness (µm)	0.156	0.23
n_{eff}	3.026	3.062
d_{eff} (pm/V) (4)	56.1	62.7
F_{eff} (µm^2) (2) with (1)	128	104
η_{nor} (%/W) (3) with (1)	103	153
F_{eff} (µm^2) (2) with (5)	101	75
η_{nor} (%/W) (3) with (5)	130	214

TABLE 1 Waveguide and conversion parameters of the optimized M-waveguide structures for the TE_0–TE_2 interaction. The refractive indices of the core are $n_{\text{core}} = 3.028$ @ $1.6\,\mu$m and $n_{\text{core}} = 3.18$ @ $0.8\,\mu$m The values of the normalized conversion efficiency η_{nor} are calculated for an interaction length of $L = 1$ cm

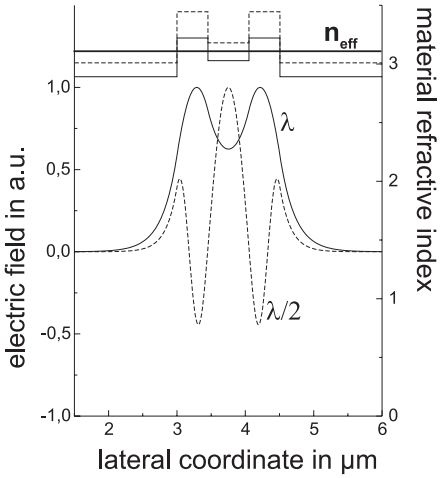

FIGURE 9 Optimized TIR coupler structure and mode fields for the TE_0–TE_4 interaction. *Solid lines*: fundamental wave at λ; *dashed lines*: harmonic wave at λ/2

waveguide approach by Chowdhury and McCaughan adapted to the AlGaAs material system. It yields a normalized conversion efficiency of $\eta_{\mathrm{nor}} = 105\%/\mathrm{W}$ (for $L = 1$ cm) and is depicted in Fig. 9.

For the fundamental wave the waveguiding is determined by the reflector layers. The effective index lies above the refractive index of the core, and the mode field consists of a supermode. For the harmonic wave the effective index lies below the refractive index of the core, and the mode field consists of a fourth-order ARROW mode. The waveguide and corresponding conversion parameters are listed in Table 2. The nonlinear overlap is less than that for the presented TE_0–TE_2 interactions, whereas the mean value of the nonlinear coefficient is higher due to the thicker reflectors with a smaller Al fraction.

However, using (1) and (3) for the waveguide optimization is a rough approximation, because the problem is separated into an effective nonlinear coefficient and an effective area. If the nonlinear overlap integral is calculated exactly by

$$K = \frac{\left| \iint_{-\infty}^{+\infty} \bar{d}(x) E_{\omega}^2 E_{2\omega} \mathrm{d}x\mathrm{d}y \right|}{\iint_{-\infty}^{+\infty} E_{\omega}^2 \mathrm{d}x\mathrm{d}y \left(\iint_{-\infty}^{+\infty} E_{2\omega}^2 \mathrm{d}x\mathrm{d}y \right)^{\frac{1}{2}}} , \tag{5}$$

with

$$\bar{d}(x) = \frac{d(x)}{d_{\mathrm{eff}}} , \tag{6}$$

different values are obtained for the quantities that characterize the conversion process. Then the waveguide configuration for the TE_0–TE_4 interaction, as shown in Fig. 9 and Table 2 (approach by Chowdhury and McCaughan adapted to AlGaAs), yields a small nonlinear overlap ($\leftrightarrow F_{\mathrm{eff}} = 6490\,\mu\mathrm{m}^2$), because the product of the electric field distributions changes sign four times across the waveguide. This results in a large reduction of the normalized conversion efficiency to $3.7\%/\mathrm{W}$. For the TE_0–TE_2 interaction the ARROW structure, as shown in Fig. 8 and Table 1, yields an effective area of $F_{\mathrm{eff}} = 101\ \mu\mathrm{m}^2$, resulting in a normalized conversion efficiency of $\eta_{\mathrm{nor}} = 130\%/\mathrm{W}$ for a device length of 1 cm. For

	TIR coupler
Core thickness (µm)	0.6
Reflector thickness (µm)	0.453
n_{eff}	3.111
d_{eff} (pm/V) (4)	80
F_{eff} (µm^2) (2) with (1)	233
η_{nor} (%/W) (3) with (1)	105
F_{eff} (µm^2) (2) with (5)	6490
η_{nor} (%/W) (3) with (5)	3.7

TABLE 2 Waveguide and conversion parameters of the optimized TIR coupler structure for the TE_0–TE_4 interaction. The refractive indices of the core are $n_{\mathrm{core}} = 3.028$ @ 1.6 µm and $n_{\mathrm{core}} = 3.18$ @ 0.8 µm. The values of the normalized conversion efficiency η_{nor} are calculated for an interaction length of $L = 1$ cm

the TE_0–TE_2 interaction the TIR coupler waveguide configuration as given in Table 1 shows an even better nonlinear overlap ($\leftrightarrow F_{\mathrm{eff}} = 75\ \mu\mathrm{m}^2$), and therefore a higher normalized conversion efficiency of $\eta_{\mathrm{nor}} = 214\%/\mathrm{W}$ for the same interaction length.

4 Conclusions

By numerical simulations we obtain simple waveguide designs based on M-waveguide structures which are usable for phase-matched SHG in AlGaAs. The total internal reflection background structure provides good confinement of the wave, while the core in the middle of the index profile causes compensation of the material dispersion. There are two relevant phase-matching points for a nonlinear interaction of a TE_0 pump field with a TE_2 or a TE_4 field of the second harmonic. For both field interactions, the waveguide parameters can be chosen either in the ARROW regime or in the coupler regime. Whereas in the ARROW case the core area determines the waveguiding, in the coupler structures with thicker reflectors the core acts as a perturbation of the overall total internal reflection structure. The differences in the waveguide geometry influence the conversion efficiency. Both the interaction overlap and the effective nonlinear coefficient are affected. Best conversion parameters are found for a coupler design of the TE_0–TE_2 interaction. The normalized conversion efficiency is $\eta_{\mathrm{nor}} = 153$ or $214\%/\mathrm{W}$ respectively for a device length of $L = 1$ cm.

The theoretical value obtained is in good correspondence with those cited in the literature for other phase-matching approaches in AlGaAs. Whereas Fiore et al. [15] report a theoretical value of $81\%/\mathrm{W}$ for a waveguide of 1.7 mm by introduction of artificial birefringence in multilayers, a comparable value of $124\%/\mathrm{W}$ is given by Yoo et al. [16] for a quasi-phase-matched AlGaAs waveguide. Eyres et al. [17] give $24\%/\mathrm{W}$ for another orientation patterned GaAs device.

For an experimental realization the slab waveguide design can be grown on GaAs substrates using standard molecular beam epitaxy (MBE). Due to the symmetry of the non-zero tensor element d_{14} of the nonlinear susceptibility of GaAs, the growth direction should be chosen in the (111) direction for a TE polarized pump field, in order to obtain second harmonic polarization in the same polarization plane. The M-waveguide designs suggested in this contribution are universally valid. They can be transferred to other material systems

and might also be used for other phase-matched, second-order processes. Therefore, the M-waveguide represents an interesting alternative device for efficient guided-wave frequency conversion.

ACKNOWLEDGEMENTS Financial support by the Volkswagen Foundation (project "Photonik I/73 883") is gratefully acknowledged. The authors would like to thank J.-P. Meyn for valuable discussions.

REFERENCES

1 P.K. Tien: Appl. Opt. **10** , 2395 (1971)
2 T. Taniuchi, K. Yamamoto: Tech. Dig. 12th Eur. Conf. Opt. Commun. **I**, 22 (1986)
3 E.J. Lim, M.M. Fejer, R.L. Byer: Electron. Lett. **25**, 174 (1989)
4 R. Regener, W. Sohler: J. Opt. Soc. Am. B **5**, 267 (1988)
5 M.A. Duguay, Y. Kokubun, T.L. Koch, L. Pfeiffer: Appl. Phys. Lett. **49**, 13 (1986)
6 Y. Kokubun, T. Baba, T. Sakaki: Electron. Lett. **22**, 892 (1986)
7 M. Mann, U. Trutschel, C. Wächter, L. Leine, F. Lederer: Opt. Lett. **16**, 805 (1991)
8 R. Freye, Th. Delonge, H. Fouckhardt: J. Opt. Commun. **16**, 42 (1995)
9 A. Chowdhury, L. McCaughan: IEEE Photon. Technol. Lett. **12**, 486 (2000)
10 B. Oster, H. Fouckhardt: IEEE Photon. Technol. Lett. **13**, 672 (2001)
11 A. Yariv, IEEE J. Quantum Electron. **QE-9**, 919 (1973)
12 S. Janz, Y. Beaulieu, A. Fiore, P. Bravetti, V. Berger, E. Rosencher, J. Nagle: Opt. Exp. **2**, 462 (1998)
13 J. Chilwell, I. Hodgkinson: J. Opt. Soc. Am. A **1**, 742 (1984)
14 T. Baba, Y. Kokubun: IEEE J. Quantum Electron. **QE-28**, 1689 (1992)
15 A. Fiore, S. Janz, L. Delobel, P. van der Meer, P. Bravetti, V. Berger, E. Rosencher, J. Nagle: Appl. Phys. Lett. **72**, 2942 (1998)
16 S.J. Yoo, R. Bhat, C. Caneau, M.A. Koza: Appl. Phys. Lett. **66**, 3410 (1995)
17 L.A. Eyres, P.J. Tourreau, T.J. Pinguet, C.B. Ebert, J.S. Harris, M.M. Fejer, L. Becouarn, B. Gerard, E. Lallier: Proc. ECIO 2001, 469 (2001)